IL NUOVO CIMENTO Vol. 35 C, N. 1 Gennaio-Febbraio 2012
DOI 10.1393/ncc/i2012-11135-7

Colloquia: LaThuile11

Scalar dark matter: A revision of the Inert Doublet Model

L. Lopez-Honorez
Service de Physique Théorique, Université Libre de Bruxelles - 1050 Bruxelles, Belgium

(ricevuto il 29 Settembre 2011; pubblicato online il 24 Gennaio 2012)

Summary. — The Inert Doublet Model (IDM) is a simple and yet very rich extension of the Standard Model which provides interesting scalar dark matter candidates. In these proceedings, we show that annihilation into 3 body final states $WW^* \to \bar{f}f'$ can significantly affect the viable parameter space of the IDM below the W threshold as well as the prospects for direct and indirect detection searches. We also show that the new viable region of the IDM between $\sim$ 80–150 GeV is already almost completely ruled out by the most recent results of the Xenon 100 experiment.

PACS 95.35.+d – Dark matter (stellar, interstellar, galactic, and cosmological).
PACS 12.60.-i – Models beyond the standard model.
PACS 12.60.Fr – Extensions of electroweak Higgs sector.

1. – Introduction

Even though dark matter accounts for about 23% of the energy density of the Universe [1], we do not yet know its true substance. Among the zoo of dark matter candidates now available in the literature, the inert dark matter particle has earned a special place as a representative candidate of weakly interacting scalar dark matter.

In the inert doublet model, a Higgs doublet H_2, odd under a new Z_2 symmetry, is added to the standard model particle content. The scalar potential of this model is given by

$$V = \mu_1^2|H_1|^2 + \mu_2^2|H_2^2| + \lambda_1|H_1|^4 + \lambda_2|H_2|^4 + \lambda_3|H_1|^2|H_2|^2 + \lambda_4|H_1^\dagger H_2|^2 + \frac{\lambda_5}{2}\left[(H_1^\dagger H_2)^2 + \text{h.c.}\right],$$

where H_1 is the Brout-Englert-Higgs doublet (referred to as Higgs in the following), and λ_i and μ_i are real parameters. Four new physical states are obtained in this model: two charged states, $H^\pm$, and two neutral ones, H^0 and A^0. We choose H^0 to be the lightest inert particle, $m^2_{H^0} < m^2_{A^0}, m^2_{H^\pm}$ and the dark matter candidate. In our study, we will use the following free paremeters: the combination $\lambda_L = (\lambda_3 + \lambda_4 + \lambda_5)/2$ corresponding to the scalar coupling of a pair of H_0 to the Higgs particle h; m_{H^0}, the H_0 mass;

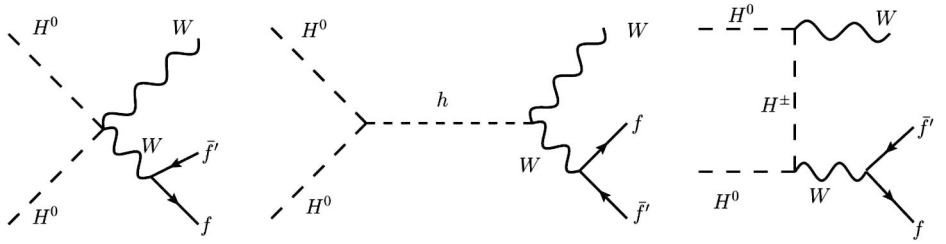

Fig. 1. – The Feynman diagrams that contribute, in the unitary gauge, to the H^0H^0 annihilation into the three-body final state $WW^* \to Wf\bar{f}'$ within the inert doublet model.

$\Delta m_{A^0} = m_{A^0} - m_{H^0}$ and $\Delta m_{H^\pm} = m_{H^\pm} - m_{H^0}$, two mass splittings between the inert scalars, and the Higgs mass, m_h. Notice that the λ_2 parameter has a small impact on the dark matter analysis. We take into account all the known theoretical and experimental constraints on this model—see [2] and [3]. This model has been extensively studied in a number of recent works (see [4] and references therein). It was shown that the dark matter relic density constraint can be satisfied for restricted values of m_{H^0}. Four viable regions can be distinguished: a small mass regime with $m_{H^0} \sim 8\,\text{GeV}$ [5,6], a large mass regime with $m_{H_0} > 500\,\text{GeV}$ [7,3,8] and two intermediate mass regime: $m_{H_0} \lesssim M_W$ [2,3] and $m_{H_0} \gtrsim M_W$ (as recently pointed out in [9]).

On general grounds annihilation of dark matter particles can receive large contributions from three-body final states consisting of a real and a virtual massive particle [10-12]. In [4], we pointed out that the annihilation into the three-body final state WW^* ($\to Wf\bar{f}'$), are important in the intermediate mass region below the W threshold. Moreover, in ref. [9], we demonstrated the existence of a new viable region of the inert doublet model featuring dark matter masses between M_W and about 160 GeV. In that mass regime, the correct relic density is obtained thanks to cancellations between different diagrams contributing to dark matter annihilation into gauge bosons (W^+W^- and Z^0Z^0). In these proceedings, we summarize the impact of the inclusion of the three-body final state WW^* on the IDM and show that the new viable region of the IDM, just above W threshold, is almost ruled out by direct detection experiments.

2. – Impact of the WW^* annihilation processes for fixed parameters

In order to clarify how important the annihilation of dark matter into WW^* ($H^0H^0 \to WW^* \to Wf\bar{f}'$) can be in the inert doublet model, we first focus on the three-body annihilation cross section $\sigma(H^0H^0 \to WW^*)$ fixing the free parameters of the model without imposing the WMAP relic abundance constraint [1]. In fig. 1, we represent the three diagrams contributing to the annihilation of dark matter into WW^*. For the range of parameters that we consider here ($m_{H_0} < m_{A_0}, m_{H_\pm}$ and $m_{H_0} \lesssim M_W$), their amplitudes depend weakly on m_{A^0} (only through the Higgs width) and on m_{H^+} (the H^+ mediated diagram is suppressed by the t-(u-)channel propagator). $\sigma(H^0H^0 \to WW^*)$ is however much more sensitive to m_{H^0}, λ_L (sign and magnitude), and m_h.

In fig. 2, the left panels compare the two- and three-body annihilation rates at low velocity, denoted by σv, for three different Higgs masses $m_h = 120$ (top), 150 (middle) and 200 (bottom) GeV. The two-body annihilation rate that has been thought to drive indirect detection processes (well) below the W threshold is $H^0H^0 \to h \to f\bar{f}$. It is

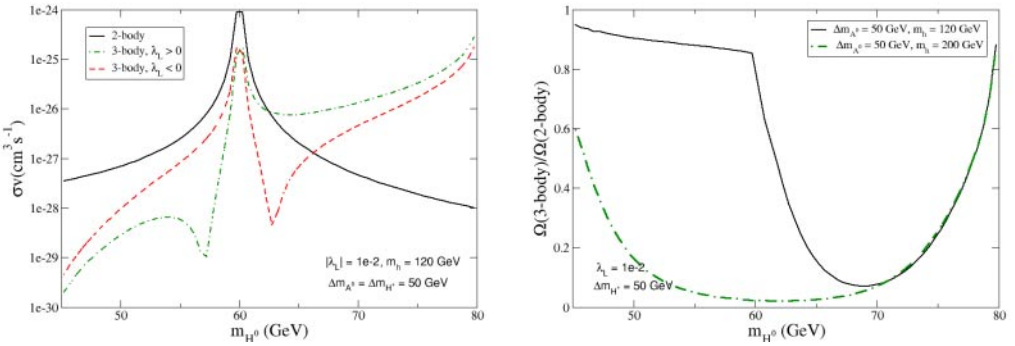

Fig. 2. – Annihilation rates and relic density ratios as a function of m_{H_0} for $|\lambda_L| = 10^{-2}$ and $\Delta m_{A^0} = \Delta m_{H^\pm} = 50\,\text{GeV}$. Left panel: Comparison between the three-body and the two-body annihilation rate, σv, as a function of the dark matter mass for the two possible signs of λ_L and $m_h = 120\,\text{GeV}$. Right panel: Ratio between the relic density including the three-body final state and the relic density for two-body final states only for $m_h = 120\,\text{GeV}$ and $200\,\text{GeV}$.

a Higgs-mediated process, whose amplitude depends on λ_L and on the Yukawa coupling of the outgoing fermions f to the Higgs. We see in fig. 2 that the three-body process can actually compete with the two-body ones. This is related to the Yukawa suppression present in $\sigma \text{v}_{\text{2-body}}$ and to the large multiplicity of final states associated with WW^* ($\to \sum_f Wf\bar{f}'$) processes. $\sigma \text{v}_{\text{3-body}}$ generically increases as m_{H^0} gets closer to M_W and its dependence in the scalar parameters λ_L, m_h is stronger around the Higgs resonance, $m_{H^0} \sim m_h/2$. More specifically, the presence of a trough in $\sigma \text{v}_{\text{3-body}}$ next to $m_{H^0} = m_h/2$ is due to the interference between the purely gauge diagram and the Higgs-mediated diagram (left and central diagrams in fig. 1). Because of such interference, the three-body cross section for $\lambda_L > 0$ (dash-dotted line) is larger than that for $\lambda_L < 0$ (dashed line) above the Higgs resonance but smaller than it below the resonance. In any case, the crucial point for us is that the three-body cross section is not negligible at all, especially next to the W threshold.

We can now compare the relic density obtained for two-body final states only (denoted as Ω(2-body)) with the one that includes the final state WW^* (denoted as Ω(3-body) and referred to as the 3-body relic density). Let us mention that for our calculations, we have used a modified version of micrOMEGAs, see [13] and references therein, in which we incorporated the annihilation into the three-body final state WW^*. To illustrate the effect of the three-body final state on the relic abundance, we show in the right panels of fig. 2 the ratio Ω(3-body)/Ω(2-body) as a function of m_{H_0} for two values of the Higgs masses $m_h = 120$ and $200\,\text{GeV}$.

A ratio equal to 1 means that the three-body process gives a negligible correction to the calculation of the relic density. Clearly, that is not the case. The ratio tends to 1 for m_{H^0} close to M_W, where the annihilation into W^+W^- is efficient, and for $m_{H^0} \ll M_W$, where the three-body annihilation is suppressed, but in the intermediate region the three-body final state plays a major role, giving rise to a correct relic density significantly smaller than the two-body one. An effect that is present for every Higgs mass and can lead to an overestimation of the predicted relic density by more than one order of magnitude. Notice that using smaller Δm_{A^0}, the coannihilation through the process $H^0A^0 \to Z^* \to f\bar{f}'$ increases the effective annihilation rate that drives the relic

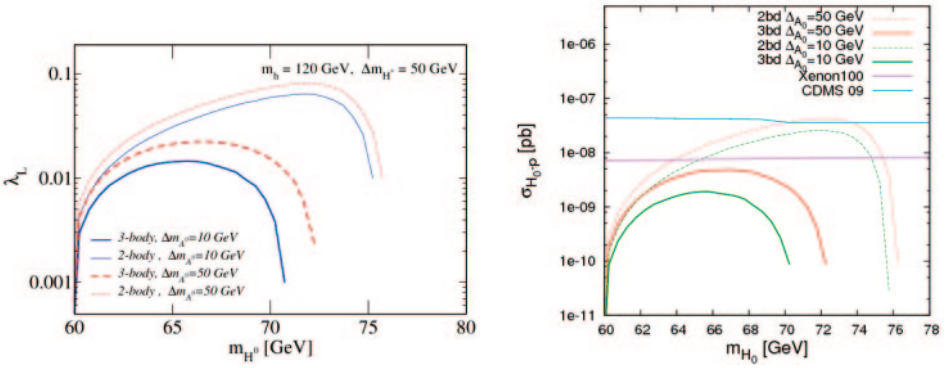

Fig. 3. – The viable parameter space for $m_h = 120\,\text{GeV}$ (left panel) and the corresponding WIMP-nucleon elastic scattering cross section (right panel). Along the lines $\Omega h^2 = 0.11$. The thick lines are the result including the final state WW^*, the thin lines correspond to 2-body final states only.

abundance. They also reduce the impact of three-body process on the relic density. It can be shown though [9] that the effect of the three-body final state remains important over a significant portion of the viable parameter space of the inert doublet model.

3. – The impact of WW^* on the viable parameter space

We can now study the impact of the three-body process on the viable parameter space, *i.e.* the parameter space determined by requiring that the predicted relic abundance be compatible with the observed density of dark matter [1]. For definiteness, we focus on $m_h = 120\,\text{GeV}$ with $\lambda_L > 0$. The left panel of fig. 3 shows the viable parameter space of the intermediate mass range of the inert dark matter model in the plane (λ_L, m_{H^0}) for $\Delta m_{H^\pm} = 50\,\text{GeV}$, and two different values of Δm_{A_0}, 10 GeV (more coannihilations) and 50 GeV. The thin lines in these figures correspond to the viable regions if only two-body final states are considered. The thick lines, on the contrary, correspond to the *genuine* viable regions, those obtained by taking into account two- and three-body final states in the calculation of the relic density. We see that, as a consequence of the three-body final state contribution to the annihilation rate of inert Higgs dark matter, the required value of λ_L is smaller at any given mass, and the maximum allowed value of m_{H^0} gets reduced by several GeVs (without taking into account cancellations, see sect. **4**). The modification of the viable parameter space, induced by the annihilation into the three-body final state WW^*, appears to be a generic feature of the inert doublet model. A feature that is present over a wide range of m_{H^0} quite independently of the other parameters of the model. As a consequence, the prospects for direct, indirect detection but also Higgs searches have to be reexamined.

In the inert Higgs model, the $H^0 N$ scattering cross section, $\sigma_{H^0 N}$, relevant for direct detection is Higgs-mediated and is proportional to λ_L^2. Given the new allowed values of λ_L that were derived above, $\sigma_{H^0 N}$ appears to be significantly reduced with respect to the two-body result used, until now, in the literature. This is illustrated in the right panels of fig. 3 where the prediction for $\sigma_{H^0 N}$ are shown along the viable lines of the inert doublet model for $m_h = 120$. For comparison, in this figure we also show the current limit from CDMS [14] and the recent results of the Xenon100 experiment [15]. Notice from

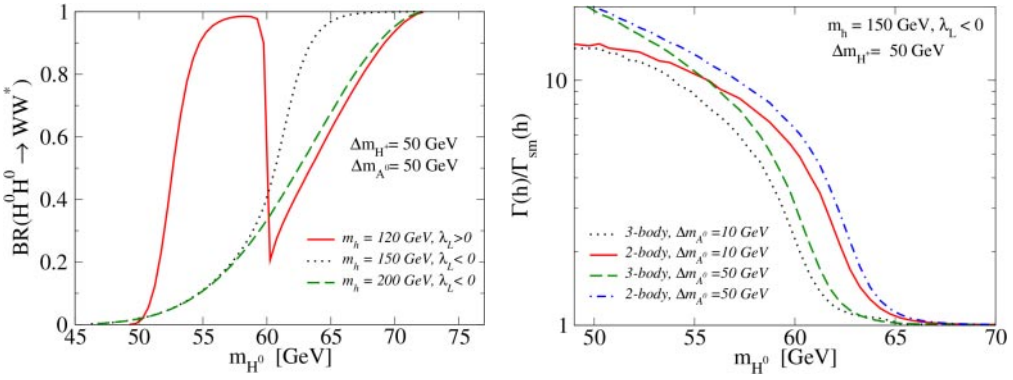

Fig. 4. – Left panel: Annihilation branching ratio into the three-body final state WW^* along the viable regions of the inert doublet model. Right panel: Ratio between the Higgs branching ratios in the inert doublet model and in the standard model along the viable regions for $m_h = 150\,\text{GeV}$. λ_L was taken to be negative and $\Delta m_{H^\pm} = 50\,\text{GeV}$.

the figure that the correct direct detection cross section can be more than two orders of magnitude smaller than the one obtained for two-body final states leading to less stringent constraints on the IDM from the present bounds set by direct detection searches.

The indirect detection signals of inert Higgs dark matter are also altered by the existence of the three-body final state WW^*. On the one hand, these signals should be now computed along new regions, due to the modified viable parameter space. On the other hand, in these new regions the annihilation cross section and branching ratios typically receive large corrections from the three-body final state WW^*. As a result, the spectrum of photons, neutrinos, positrons and antiprotons expected from inert Higgs annihilation will be different, changing its indirect detection prospects. In the left panel of fig. 4, we show that the three-body final state WW^* becomes dominant over a sizeable region of the viable parameter space.

In the inert doublet model, the Higgs boson can decay also into H^0H^0 and A^0A^0, increasing the Higgs decay width and modifying its branching ratios. The contribution to the Higgs decay with from the decay into the inert scalars is proportional to λ_L^2, so that it will be affected by the three-body final state WW^* via the new viable parameter space. In the right panel of fig. 4, we illustrate for $m_h = 150\,\text{GeV}$ how the Higgs decay width can be modified when including the three-body final state in the determination of the relic abundance. This should be taken into account for Higgs searches at colliders.

4. – Cancellations in the $m_{H^0} > M_W$ regime

Above the W threshold, $m_{H^0} > M_W$, dark matter annihilation into W^+W^- becomes kinetimatically allowed, with the result that the total annihilation cross section tends to be rather large. Typically, the pure gauge contributions (*i.e.* setting all the inert scalar couplings to zero) give rise to annihilation cross sections much larger than those required to obtain the correct relic density ($\sigma \text{v} \sim 3 \times 10^{-26}\,\text{cm}^3/\text{s}$), so that it seems difficult to satisfy the dark matter constraint in this mass range. In ref. [9] we have shown([1]) that

([1]) See also [16] and [4].

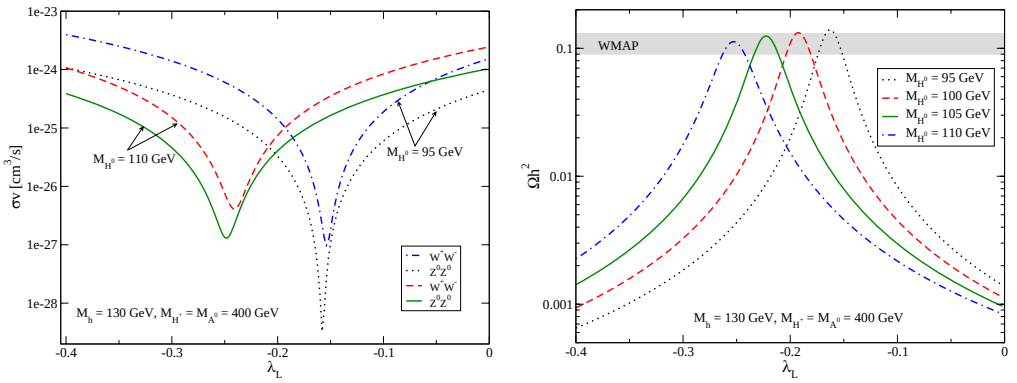

Fig. 5. – Left panel: The dark matter annihilation cross section (at low velocity) into W^+W^- and Z^0Z^0 as a function of λ_L for two different values of m_{H^0}: 95 GeV and 110 GeV. Right panel: Relic density.

taking advantage of the interference among the different diagrams that contribute to dark matter annihilation into gauge bosons, it is possible to satisfy the relic density constraint for $m_{H^0} \gtrsim M_W$. Thus, opening up a new viable region of the inert doublet model.

It is easy to show that a cancellation between the diagram contributing to the annihilation into two gauge bosons occurs for $\lambda_L \approx -2(m_{H^0}^2 - (M_h/2)^2)/v^2$. In the following, we refer to that condition as the cancellation condition. Hence, cancellations take place for $\lambda_L > 0$ if $m_{H^0} < M_h/2$ and for $\lambda_L < 0$ if $m_{H^0} > M_h/2$. Notice also that the cancellation condition is the same for both final states, W^+W^- and Z^0Z^0, indicating that both processes will be simultaneously suppressed. Suppressing the annihilations into W^+W^- and Z^0Z^0 is not enough to ensure a small dark matter annihilation cross section. In addition, we must make sure that annihilation into the other possible final states is not kinematically allowed. In the following, we will see that the viable models taking advantage of the cancellations feature $m_{H^0} < M_h, m_t$.

5. – Examples

The cancellation effects we have described are illustrated in the left panel of fig. 5, which shows the dark matter annihilation cross sections into W^+W^- and Z^0Z^0 as a function of λ_L. For this figure we set $M_h = 130\,\text{GeV}$, $M_{H^\pm} = M_{A^0} = 400\,\text{GeV}$, and we consider two different values of m_{H^0}: 95 GeV and 110 GeV. The cancellation condition tells us that the cancellations should take place for negative values of $\lambda_L = -0.16$ and -0.26, respectively, which is in good agreement with the full numerical treatment of the annihilation cross section. We observe that the larger m_{H^0} the larger the value of $|\lambda_L|$ required to obtain cancellations.

Since $\Omega h^2 \propto 1/\sigma\text{v}$, we expect these cancellations in the annihilation cross section to increase significantly the inert Higgs relic density, opening up the possibility of finding viable models for $m_{H^0} \gtrsim M_W$. This is illustrated in the right panel of fig. 5.

6. – The new viable region and the constraints from direct detection searches

In ref. [9], we have performed a systematic analysis of this new viable region of the parameter space using a Markov Chain Monte Carlo (MCMC). The left panel of fig. 6

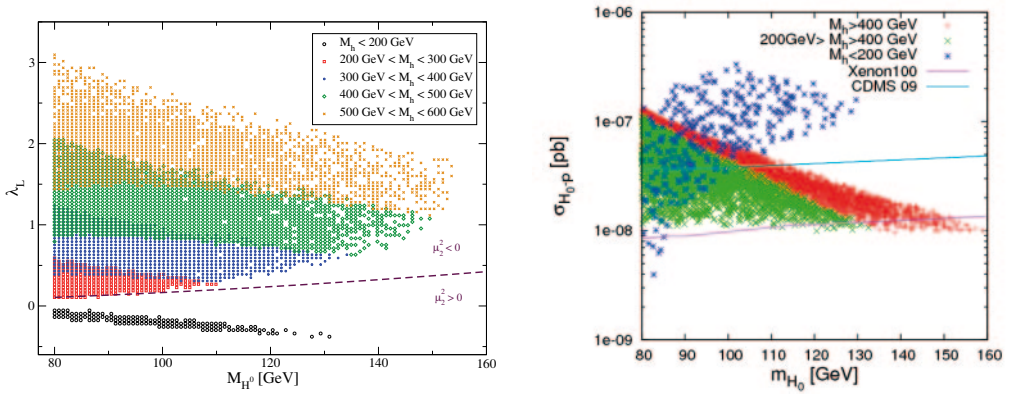

Fig. 6. – (Colour on-line) Left panel: The new viable region projected on the plane (m_{H^0}, λ_L). The different symbols (and colors) distinguish among the possible ranges of M_h. The dashed line is the contour $\mu_2^2 = 0$. Right panel: scattering cross section relevant for direct detection searches.

shows the new viable region of the inert doublet model in the plane (m_{H^0}, λ_L). Notice that the value of m_{H^0} over the new region extends from M_W up to about 160 GeV. In λ_L, the range of possible values extends from -0.5 to about 3.0. A sharp contrast is observed between the models with $\lambda_L < 0$ and those with $\lambda_L > 0$. In the former case ($\lambda_L < 0$), the maximum value of m_{H^0} is about 130 GeV and the Higgs boson is necessarily light, $M_h < 200$ GeV, as cancellations occur for $m_{H^0} > M_h/2$. In the latter case ($\lambda_L > 0$), the maximum value of m_{H^0} can be larger, strongly depending on the range of Higgs masses. Thus, for 200 GeV $< M_h <$ 300 GeV the maximum m_{H^0} is only about 110 GeV whereas it can reach almost 160 GeV for the largest Higgs masses, $M_h > 500$ GeV. It is also apparent from the figure, that for $\lambda_L > 0$ the larger the Higgs mass the larger λ_L must be.

In the inert Higgs model, the $H^0 p$ scattering process relevant for direct detection is Higgs-mediated and its cross section, $\sigma_{H_0 p}$, is directly proportional to the square of λ_L. Given the rather large values of λ_L we found, we foresee that $\sigma_{H_0 p}$ will be significant over the entire new viable region. In the right panel of fig. 6, we show the spin-independent dark matter-nucleon cross section, $\sigma_{H_0 p}$, as a function of m_{H^0} for our sample of models. $\sigma_{H_0 p}$ lies in a narrow range between 3×10^{-7} and 10^{-8} Pb. In this figure we show the constraints resulting from the present experimental (CDMS experiment [14] and Xenon100 [15]). We see that the very last results of the Xenon100 experiment exclude almost the entirety of this new viable region [15].

7. – Conclusions

We studied the impact, on the phenomenology of the inert doublet model, of dark matter annihilation into the three-body final state WW^* and of cancellations among the diagrams contributing to the annihilation just above the W threshold. The annihilation cross section into WW^*, $\sigma(H^0 H^0 \to WW^*)$, was shown to dominate the total dark matter annihilation cross section over a relevant portion of the parameter space. In consequence, the viable H_0-coupling to the Higgs (λ_L) can be reduced by one order of magnitude. This implies that the scattering cross section ($\propto \lambda_L^2$) relevant for direct

detection searches can become two orders of magnitude smaller. Moreover, concerning the new viable parameter space of the IDM just above the W threshold, we have shown that the last results of the Xenon 100 experiment excluded almost all the models with masses $m_W < m_{H^0} < 160\,\mathrm{GeV}$.

* * *

I would like to thank the organizers of La Thuile 2011 for giving me the opportunity to present this work at the conference. The results presented in these proceedings were originaly obtained in collaboration with Carlos E. Yaguna in ref. [4] and in ref. [9] I was supported in part by the IISN and by Belgian Science Policy (IAP VI/11).

REFERENCES

[1] Komatsu E. *et al.*, *Astrophys. J. Suppl.*, **180** (2009) 330.
[2] Barbieri Riccardo, Hall Lawrence J. and Rychkov Vyacheslav S., *Phys. Rev. D*, **74** (2006) 015007.
[3] Lopez Honorez Laura, Nezri Emmanuel, Oliver Josep F. and Tytgat Michel H. G., *JCAP*, **0702** (2007) 028.
[4] Lopez Honorez Laura and Yaguna Carlos E., *JHEP*, **09** (2010) 046.
[5] Hambye Thomas and Tytgat Michel H. G., *Phys. Lett. B*, **659** (2008) 651.
[6] Andreas Sarah, Hambye Thomas and Tytgat Michel H. G., *JCAP*, **0810** (2008) 034.
[7] Cirelli Marco, Fornengo Nicolao and Strumia Alessandro, *Nucl. Phys. B*, **753** (2006) 178.
[8] Hambye T., Ling F. S., Lopez Honorez L. and Rocher J., *JHEP*, **07** (2009) 090.
[9] Lopez-Honorez Laura and Yaguna Carlos E., *JCAP*, **01** (2011) 002.
[10] Yaguna Carlos E., *Phys. Rev. D*, **81** (2010) 075024.
[11] Chen Xue-lei and Kamionkowski Marc, *JHEP*, **07** (1998) 001.
[12] Hosotani Yutaka, Ko Pyungwon and Tanaka Minoru, *Phys. Lett. B*, **680** (2009) 179.
[13] Belanger G., Boudjema F., Pukhov A. and Semenov A., *Comput. Phys. Commun.*, **180** (2009) 747.
[14] Ahmed Z. *et al.*, Results from the Final Exposure of the CDMS II Experiment (2009).
[15] Aprile E. *et al.* (XENON100 Collaboration), *Phys. Rev. Lett.* **107** (2011) 131302, arXiv:1104.2549
[16] Lundstrom Erik, Gustafsson Michael and Edsjo Joakim, *Phys. Rev. D*, **79** (2009) 035013.